Anal. Methods Environ. Chem. J. 8 (1) (2025) 26-38

AMECJ

Research Article, Issue 1
Analytical Methods in Environmental Chemistry Journal
Journal home page: www.amecj.com/ir

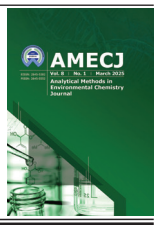

Determination and removal of methylene blue dye via photodegradation using titanium dioxide nanoparticles from watermelon rind

Mohamed Abdelkalik Hussain[a,*] and Wadhah Naji Al Sieadi[b]
[a]*Department of Chemistry, College of Science, University of Baghdad, Baghdad, Iraq*
[b]*Department of Chemistry, College of Science, University of Baghdad, Baghdad, Iraq*

ARTICLE INFO:
Received 2 Dec 2024
Revised form 4 Feb 2025
Accepted 30 Feb 2025
Available online 30 March 2025

Keywords:
Green synthesis,
TiO_2NPs,
Watermelon rind,
Methylene blue dye,
Sol-gel method

ABSTRACT
Water pollution poses significant threats to the environment and human health, applications of photodegradation technology offer a promising solution for mitigating these impacts by utilizing light energy to break pollutants; this technology can effectively clean contaminated water, contributing to a sustainable challenge and enhanced the practicality and efficiency of photodegradation systems. This study compares the photodegradation efficiency of (20 ppm, pH = 6.4) methylene blue dye (MB) under three different types of ultraviolet (UV) irradiation light sources, which are UV type A (365 nm), UV type B (311 nm), UV type C (254 nm) by using new home-made photoreactor. The photodegradation activity of this system comprises various conditions, first on circulation of MB dye in the system without irradiation or adding catalytic, when irradiation MB dye with UV-A, UV-B, and UV-C light sources with circulation, finally, the effect of adding 0.05 g of green synthesis of titanium dioxide nanoparticles (TiO_2NPs) by using watermelon rind extract with irradiation in the system. Different percentage of MB dye removal was reported. The prepared catalytic TiO_2NPs were characterized using ultraviolet−visible spectroscopy (UV-Vis), Fourier transform infrared spectroscopy (FTIR), scanning electron microscope (SEM), energy dispersive analysis (EDX), X-ray spectroscopy (XRD), and atomic force microscopy (AFM). High photodegradation performance was reported under UV-C and UV-B irradiation of MB dye in 90 minutes.

1. Introduction

Nanotechnology science refers to any product or device created by matter manipulated by controlling atoms and molecules at the nanoscale [1]. These materials are known as nanomaterials or nanoparticles (NPs), with no more than 100 nanometers thick in at least one dimension of materials or molecules at the nanoscale. These materials promise great promise for a scientific career when applied to industries like sports, healthcare, and electronics [2,3]. The field of inorganic nanoparticles has been developed in recent years. Metal nanoparticles differentiate from bulk with their physical and chemical properties, including their morphology and geometry, size and distribution, catalytic activity, and magnetic properties. This leads to broad fields of application in biomedical, electronics, environment, and air pollution [4,5]. Different chemical, physical, and biological methods produce metal nanoparticles. The chemical and

*Corresponding Author: Mohammed Abdelkalik Hussain
Email: muhamedabdelkalik@gmail.com
https://doi.org/10.24200/amecj.v8.i01.362

physical methods have their drawbacks, with hazardous products and poisonous creation products [6,7]. Biosynthesis approaches with low-cost, environmentally friendly methods, with one step to generate metal NPs, and using plant parts as a starting point such as (seeds, roots, and fruits) [8,9], or microorganisms which are used in green synthesis of metal nanoparticles [10,11] which contain bioactive agents such as fungi, yeasts, and bacteria [12-14]. A plant extract is used to produce NPs on a large scale, which is cost-effective, simple, and safe. Plant extract contains bioactive compounds that play different roles in green synthesis methods as capping, stabilizing, and reducing agents [15,16], with compounds such as saccharides [17], vitamins [18], antioxidants [19], alkaloids [20], flavonoids [21], as well as various proteins, amino acids, and enzymes [22]. Watermelon fruit (Citrullus lanatus) is one of the most consumed worldwide [23], but only the red flesh is eaten; the green rind is always discarded to waste. However, the rinds contain various bioactive components, proteins, carotenoids, citrulline, pectin, and cellulose [24,25]. Also, it contains soluble carbohydrates up to (45-65%), carotenoids, alkaloids, saponin, and phytates [26]. WMRs also contain various proteins (15-50%), including prolamin, glutelin, albumin, and globulin. Also, it is considered a good source of vitamin B-complex (B_1, B_2, B_3, B_6, and B_{12}) [27]. Water pollution nowadays receives global attention due to organic contaminations [28,29], which cannot be isolated with conventional methods. An increase in pharmaceutical concentration, especially using amino acid products, which affects plants and other living organisms [30-32]. Due to the photocatalytic technology based on the ultraviolet spectrum and TiO2NP substances [33,34], which undergo the generation of reactive oxygen species (ROS), which is considered the key oxidant that decomposes water pollutants [35]. TiO_2NPs are known for low cost, high stability photocatalytic, and non-toxicity. Also, TiO_2NPs are known for one drawback, which is a large band gap in the visible spectrum [36]. Several chemical and physical methods are reported to remove dyes and organic pollutants from water, such as photocatalysis, coagulation-flocculation, adsorption, membrane separation, and electrochemical processes. Among all these methods, photocatalysis has been reported as cheaper, more effective, and preferred over other methods due to its simple design, operation, energy efficiency, eco-friendliness, and cost-effectiveness. Other methods also focus on changing the pollutants from an aqueous solution to a solid state. In contrast, photocatalysis focuses on the degradation of contaminants by an advanced oxidation process on the catalyst's surface [37–40]. The present work reports the degradation of methylene blue dye by photocatalytic method using TiO_2NPs as a photocatalyst and irradiation of different ultra-viable light sources, such as UV-A, UV-B, and UV-C.

2. Materials and Methods

2.1. Chemicals and Materials

Titanium tetrachloride (TiCl4, 99.99%, CASN.: 7550-45-0) was supplied from Sigma Aldrich, America. Methylene blue dye ($C_{16}H_{18}ClN_3S$, ≥95%, CAS N.: 61-73-4) was bought from Merck, America. Ammonia (≥10%, CASN.: 1336-21-6) bought from Prolabo, Canada. All experiments include using deionized water (DW Millipore).

2.2. Preparation of Watermelon rinds Aqueous

Several watermelons are bought from the market; the rinds are separated and washed with water to remove all remaining parts for several days. The rinds were kept in a dark place to dry. The next step was to use a grinder from Al saif-elec., model HM-917, and the dried rinds ground to powder. To prepare the aqueous solution of watermelon rind, 5.0 g of powder was added to 100 mL DW, the mixture was heated using a stirrer hot plate, the temperature kept under 80 ^{0}C, stirring at 200 rpm for 30 minutes, and a green solution was obtained, the aqueous cooled and filtered, stored in a dark brown bottle.

2.3. Preparation of green TiO_2 NPs by the Sol-Gel

To prepare TiO2NPs by sol-gel method, (100ml) of green watermelon rinds were heated and stirred with a hot plate to 70 0C, then (100 mL) of (0.5M) TiCl4 solution was added. The mixture was kept to reach the wanted temperature, a dropwise of ammonia solution was added, and the mixture color changed from white-green to yellow color after (60) minutes; the mixture cooled down, centrifuged, dried, and ground with crystal mortar to obtain the TiO_2NPs powder. The last step, purification, is done by calcinating the powder in the furnace at (400°C) to remove water moisture for three hours and oxidize the entire TiO_2NPs to powder (Fig. 1). The TiO_2NPs characterized by AFM, SEM, FTIR, UV-vis spectrum, XRD, and EDAX.

2.4. Photoreactor and UV light sources

A photoreactor instrument designed to bring photons to reactant is known as a photoreactor; the device consists of a frame bought from the market, attached to a diaphragm pump 24V.16L^{-1} min^{-1}. The frame connected to the ultraviolet chamber barrel consists of a high-quality tube of quartz for UV-light sources, which are (T5 8W) UV-A (365 nm), (T5 8W) UV-B (311 nm), and (T5 8W) UV-C (254 nm). A water cartridge with 10 inches where used, plastic tubes with connectors used to close the system flow. All UV-light sources were bought from the Coospider quartz ultraviolet lamp, 220v, China, as shown in Figure 2.

Fig. 1. Sol-Gel method for green synthesis of TiO_2NPs

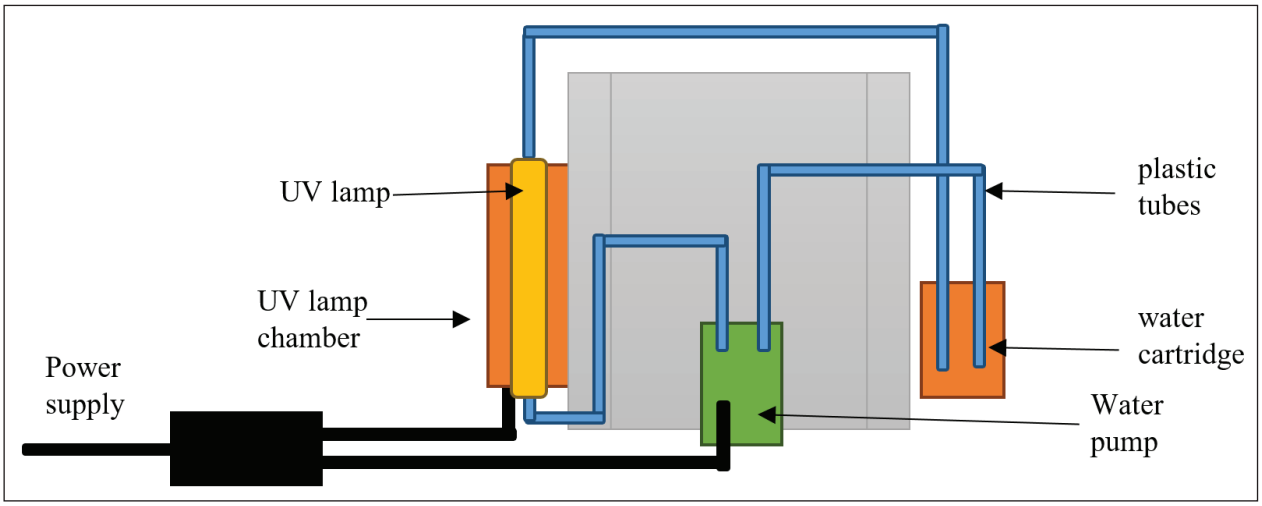

Fig. 2. Photoreactor system design

2.5. The procedure of photodegradation

To ensure the solution flow in the photoreactor device, (320 mL) of methylene blue with concentration (20 mg L^{-1},, PH = 6.4) was selected. An experiment was done to show the impact on MB circulation in the photoreactor. To study the effect of irradiation of three UV lamps, which are UV-A, UV-B, and UV-C, on the circulation of MB in the photoreactor, a set of experiments was done to show the effect. The last set of experiments was done to show the impact of loading (0.05 g) of TiO_2NPs with irradiation with three UV-lamps for degradation of MB, with these set of experiments and to ensure the adsorption-desorption equilibrium of MB on the surface of TiO_2NPs, after adding (0.05 g) of the catalyst, the solution kept for (15) minutes in a dark place. In all experiments, a sample of (2.5 mL) was first collected from the photoreactor; after irradiation started, the sample was collected every (15) minutes using a pipette, and all experiments were done in (90) minutes.

2.6. Instrument and principle of operation

Ultraviolet(UV)radiationisaformofelectromagnetic radiation with shorter wavelengths than visible light; there are three types of UV rays: UV-A, UV-B, and UV-C. To investigate the photodegradation of MB dye, a UV-Vis spectrophotometer with a double beam was used for its capability to analyze the absorption and transmission of light with the dye and degradation products, as this technique provides information about electronics transition and understand the mechanism of degradation and efficiency of the photocatalyst. This instrument is based on the interaction between light and matter; as light passes through a molecule of MB dye, it causes vibration to this molecule, and the wavelength of this absorbed light is called absorption maximum, which can identify the changes in the reaction, the instrument consists of light source which provides illumination at specific wavelength, a monochromator used to select the wavelength, a detector to measure the intensity of light passes through the sample, and a data recorder to record the absorbance or transmission of the light[41].

2.7. Photodegradation kinetic study

The photocatalytic study of TiO_2NPs was tested, and the photodegradation rate of MB dye was calculated by Equation 1 [42,43].

$$\text{MB Degradation (\%)} = \frac{A0-At}{A0} \times 100 \quad \text{(Eq.1)}$$

Where A0 is the absorbance of initial MB; At is the absorbance of the solution after irradiation at time t. According to the first-order kinetics reaction, rate constant k (min^{-1}) was determined using the following relation Equation 2[44,45]. C_0 and C_t are concentrations at the beginning, and at a particular time, t is the irradiation time.

$$\ln\left(\frac{Ct}{C0}\right) = -kt \quad \text{(Eq.2)}$$

2.8. Characterization of Titanium oxide nanoparticles

A BOYN D8000 double-beam UV−vis spectrophotometer (China) was used to identify the compounds' functional groups. The Naio AFM atomic force microscopy model Nano surf AG, Switzerland, measured the surface roughness and mean diameters. Environmental scanning electron microscopy (ESEM) and Energy-dispersive X-ray spectroscopy (EDX) were used for element analysis by Tescan Mira with a resolution of 1.2 nm at 30 kV and 2.3 nm at 3.0 kV. FTIR analysis was performed to measure the absorbances of methylene blue dye (Vertex-80v FTIR spectrometer with a frequency range from 4000–400 cm^{-1}). An XRD persee, China, XD_3 (X-ray diffractometer) was carried out on TiO_2NPs powder to identify the structure and the composition, the range -40-90° at a scanning speed 0.125°-120°min^{-1}, step size of 0.00025° with scanning radius 180 mm.

3. Results and discussion

3.1. Morphological analysis

3.1.1.Scanning Electron Microscope and Energy Dispersive Analysis of X-ray

To characterize the surface morphology of TiO_2NPs prepared by green synthesis, Figure 3

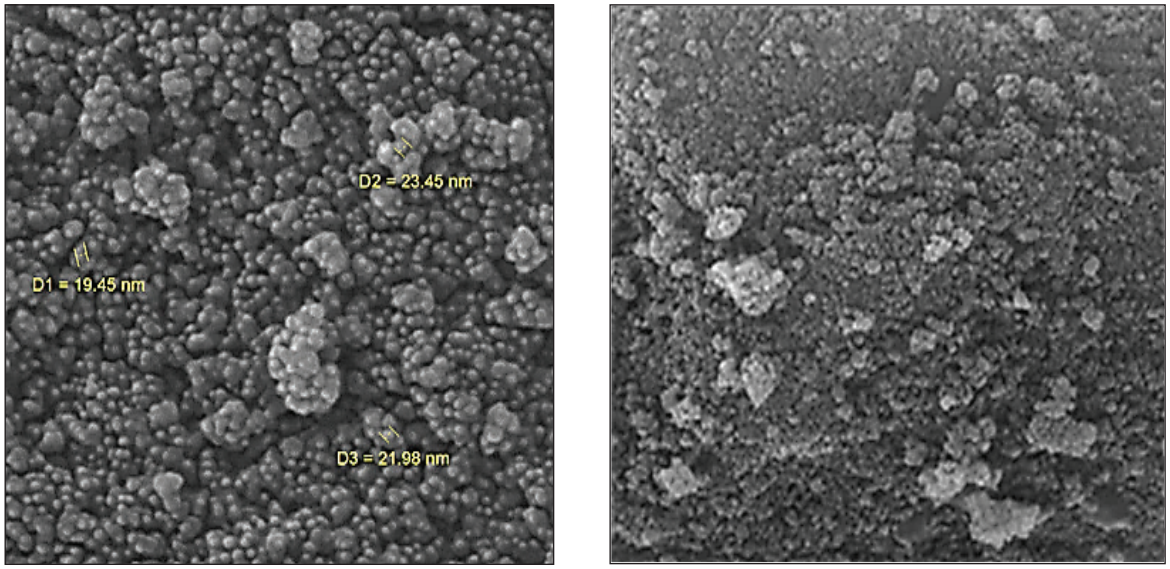

Fig. 3. SEM images of TiO_2NPs view field (left) 200 nm and (right) 1µm

(left) and (right) show the SEM images. The results of these images show the non-uniform distribution of TiO_2NPs, consisting of single particles or clusters with an average size (21 nm) diameter. Also, it is shown from a closer view that the rough surface's slight agglomerations due to high calcination temperature accelerate the crystal growth of TiO_2NPs.

Figure 4 shows an EDAX analysis used to prepare TiO2NPs. The results are described in Table 1, which shows the atomic percentage of oxygen and titanium-grown nanoparticles. This can conclude the right ratio of titanium and oxygen with 1:2. The spectra show different elements from the watermelon rind compounds, as shown in Table 1.

3.1.2.X-ray diffraction (XRD)

Figure 5 shows the results of analyzing the X-ray spectra and studying the structure and crystallization of TiO_2NPs, starting with the Match phase analysis software.

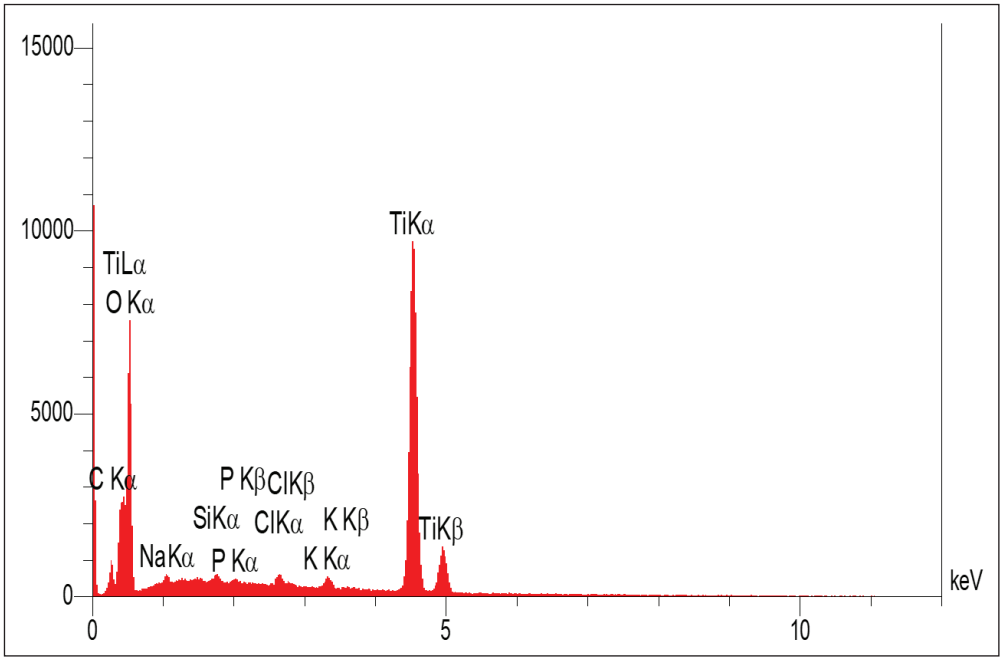

Fig. 4. TiO_2NPs EDAX spectrum

Table 1. Chemical composition of green TiO_2NPs in terms of weight and atomic percentage from (EDAX) measurement

Elements	Weight percentage (Wt. %)	Atomic percentage (%)
C	4.21	7.39
O	54.22	71.39
Na	3.18	2.92
Si	1.67	1.32
P	1.44	0.98
Cl	2.11	1.25
K	2.00	1.08
Ti	31.08	13.76
Total	100.00	100.00

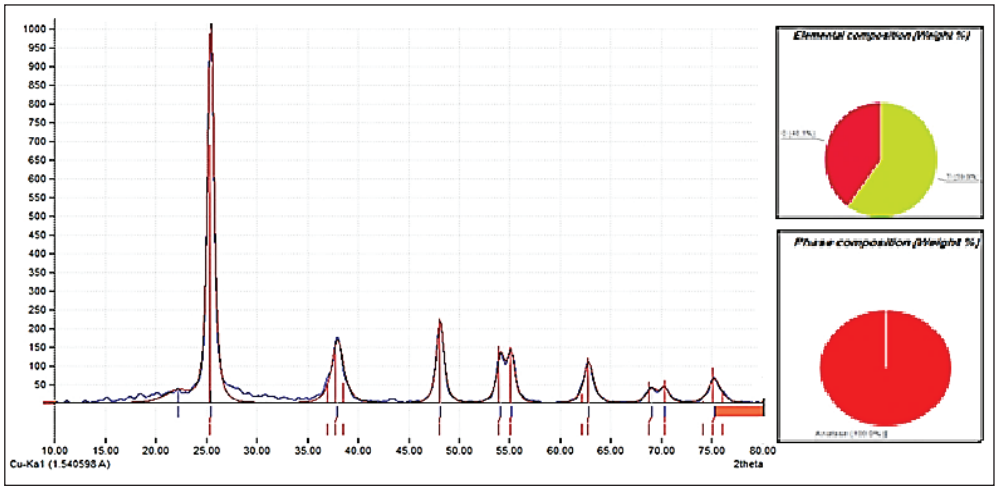

Fig. 5. XRD pattern of green synthesis TiO_2NPs

The diffraction peaks sharp spectrum appeared at 2θ = 22.20°, 25.45°, 38.00°, 48.15°, 54.13°, 55.13°,62.83°, 69.05°, 70.30°, and 75.25°. The spectrum matches with anatase phase patterns of TiO_2NPs from (COD card No. 96-901-5930) [46], with a tetragonal crystal plane and average crystallite size for the TiO_2NPs estimated according to the Debye–Scherrer's Equation 3 [47].

$$D = \frac{K*\lambda}{\beta * \mathrm{Cos}\,\theta} \qquad \text{(Eq.3)}$$

Where K represents the Scherrer constant (0.94), D is the nanoparticle crystalline size, λ is the X-ray wavelength (1.54 A°), θ is the Bragg's diffraction angle, and β is the peak width at half maximum. The average particle size has been calculated in Match software to be (26.69 nm) as shown in Figure 6.

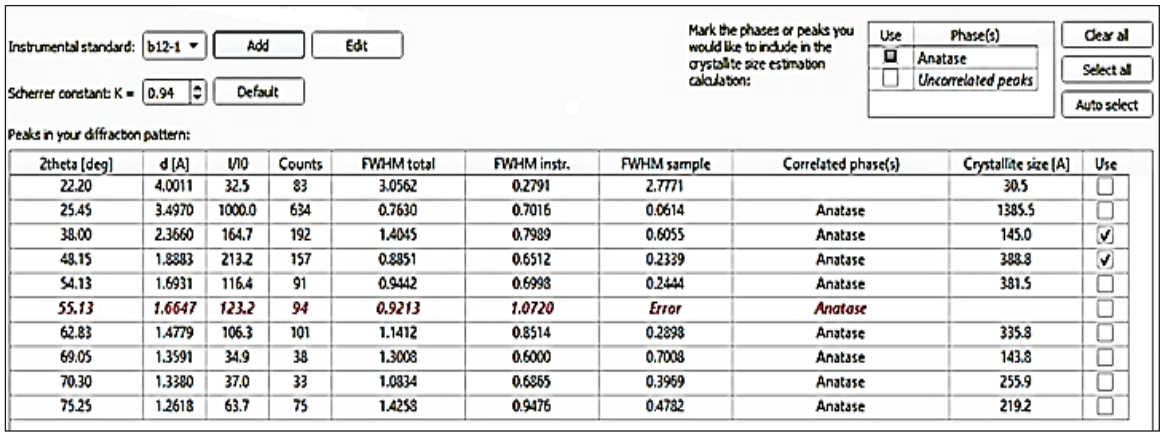

2theta [deg]	d [A]	I/I0	Counts	FWHM total	FWHM instr.	FWHM sample	Correlated phase(s)	Crystallite size [A]	Use
22.20	4.0011	32.5	83	3.0562	0.2791	2.7771		30.5	☐
25.45	3.4970	1000.0	634	0.7630	0.7016	0.0614	Anatase	1385.5	☐
38.00	2.3660	164.7	192	1.4045	0.7989	0.6055	Anatase	145.0	☑
48.15	1.8883	213.2	157	0.8851	0.6512	0.2339	Anatase	388.8	☑
54.13	1.6931	116.4	91	0.9442	0.6998	0.2444	Anatase	381.5	☐
55.13	*1.6647*	*123.2*	*94*	*0.9213*	*1.0720*	*Error*	*Anatase*		☐
62.83	1.4779	106.3	101	1.1412	0.8514	0.2898	Anatase	335.8	☐
69.05	1.3591	34.9	38	1.3008	0.6000	0.7008	Anatase	143.8	☐
70.30	1.3380	37.0	33	1.0834	0.6865	0.3969	Anatase	255.9	☐
75.25	1.2618	63.7	75	1.4258	0.9476	0.4782	Anatase	219.2	☐

Fig. 6. TiO_2NPs Crystallite size calculation

3.1.3. FTIR spectroscopy study

The FTIR spectroscopy of both watermelon rind and prepared TiO_2NPs powders was carried out to determine functional groups as shown in Figure 7. TiO_2NPs spectra (a and b) show three spectrum peaks, the observed peaks at 3452.43 cm^{-1} and 3431.13 cm^{-1}, which are stretching vibration asymmetric and symmetric attributed to the hydroxyl group in (Ti-OH) [48]. The band observed peak in 1618.17 cm^{-1} attributed to the binding vibration of the (OH) group in the water molecule, which adsorbed on the surface of TiO_2NPs [49,50], the peaks at the broadband from 800 to 400 cm^{-1} region is attributed to the Ti-O stretching and Ti-O-Ti vibration absorption from the anatase TiO_2NPs [51,52].

3.1.4. Atomic force microscopy (AFM)

AFM carried out the topography analysis phases of TiO_2NPs. The results show spherical nanoparticles. An image topographic roughness inspection showed an average size of 9nm, as shown in Figure 8.

3.2. Photodegradation Studies

3.2.1. Absorption of MB dye

The concentration of the experimental part chosen 20ppm (6×10^{-5}M) at 662 nm wavelength and (0.680) absorbance as shown in Figure 9, by reference to Beer's law, this concentration of 20ppm which lies between (0.2-0.7) absorbances with least errors and best range for measurements [53].

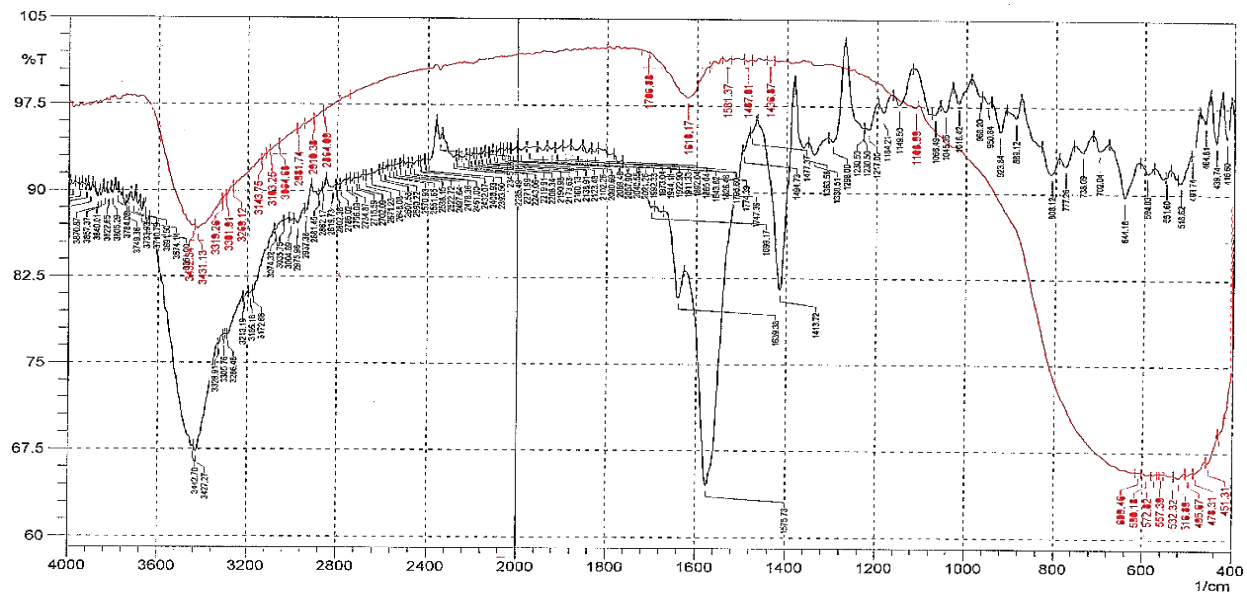

Fig.7. FTIR pattern (a) green synthesis TiO_2NPs (b) watermelon rind

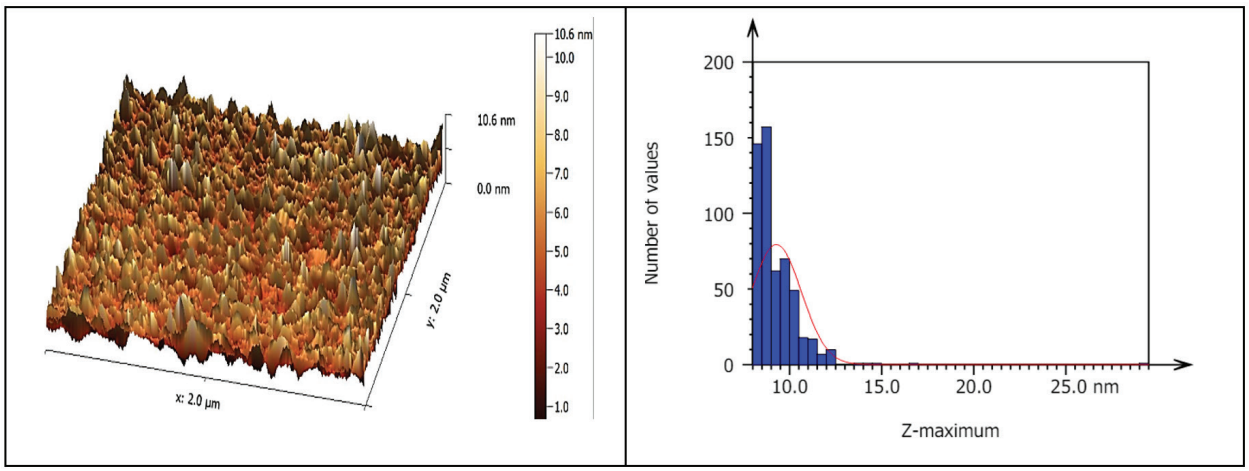

Fig. 8. TiO_2NPs Atomic force microscopy analysis

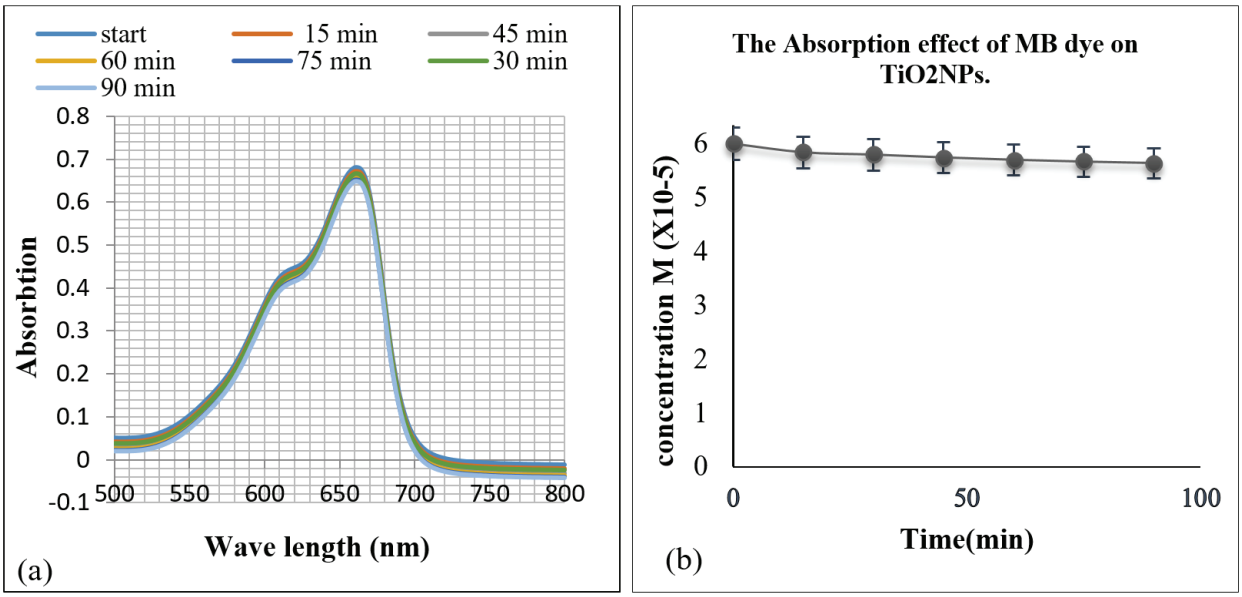

Fig. 9. UV-Vis of MB (**a**) Absorbance vs wavelength (nm), (**b**) Concentration vs time

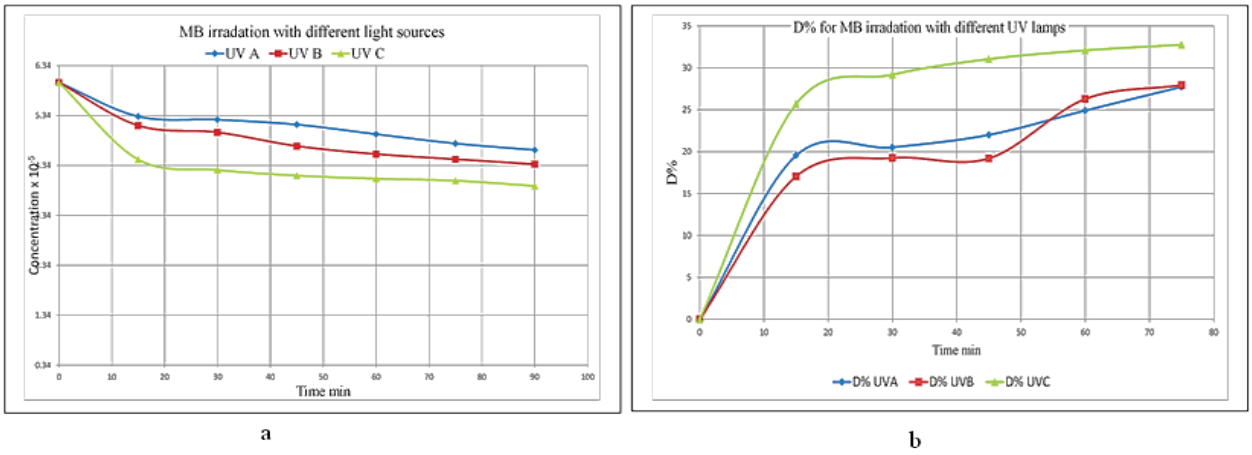

Fig. 10. (a) MB irradiation with different UV-light sources, (b) D% for MB irradiation with different UV lamps, both experiments ([MB] = 20 ppm; TiO_2NPs loading = none)

3.2.2.Irradiation of MB dye with different UV-light sources

Irradiation of MB dye with different lamps (UV-A, UV-B, UV-C) without loading photocatalyst: All these experiments show the MB decreasing in concentration with time in different percentages. Also, the photodegradation process increases with different percentages, as shown in Figures 10 and b. The results show that photodegradation for UVC = 34%, and both UVB and UVA results are 29%.

3.2.3. Photocatalyst loading for photodegradation of methylene blue

The photodegradation of methylene blue with loading (0.05g) TiO_2NPs photocatalyst has been carried out in (90) minutes with irradiation by three different UV lumps, which are UV-A (365 nm), UV-B (311nm), UV-C (254 nm), as in Figure11a, which indicate the decrease of MB dye concentration with time. UV-C reaches 99.9% degradation of MB dye after 75 minutes, while UV-B reaches 96% degradation, and UV-A reaches 50% degradation

after 90 minutes. Figure 11b shows Regression correlation values R2 for each UV tube, UV-A, UV-B, and UV-C. Figures 11c and 11d show that the degradation percentage increases (D%), and all experiments were done in (90) minutes.

The photodegradation of MB dye with UV-C is faster than that with UV-B and UV-A, indicating its photolysis capability, as it has a shorter penetration wavelength and high energy level. The photodegradation kinetic study follows a first-order reaction [54,55]. A graph of ln(C0/Ct) against time was plotted, as shown in Figure 11b, with a high regression correlation value.

4. Conclusion

This study shows the easy procedure to produce TiO_2NPs by the sol-gel method, which was successfully prepared using watermelon rinds for the green synthesis method. The critical role of green synthesis is to prepare metal nanoparticles with their advantages and acceptances in wastewater treatment and for the environment. Photodegrading using semiconductor TiO_2NPs, with a new photoreactor system design, is highly effective in degrading methylene blue dye under different ultraviolet light irradiation. This process can break down harmful organic compounds into less toxic

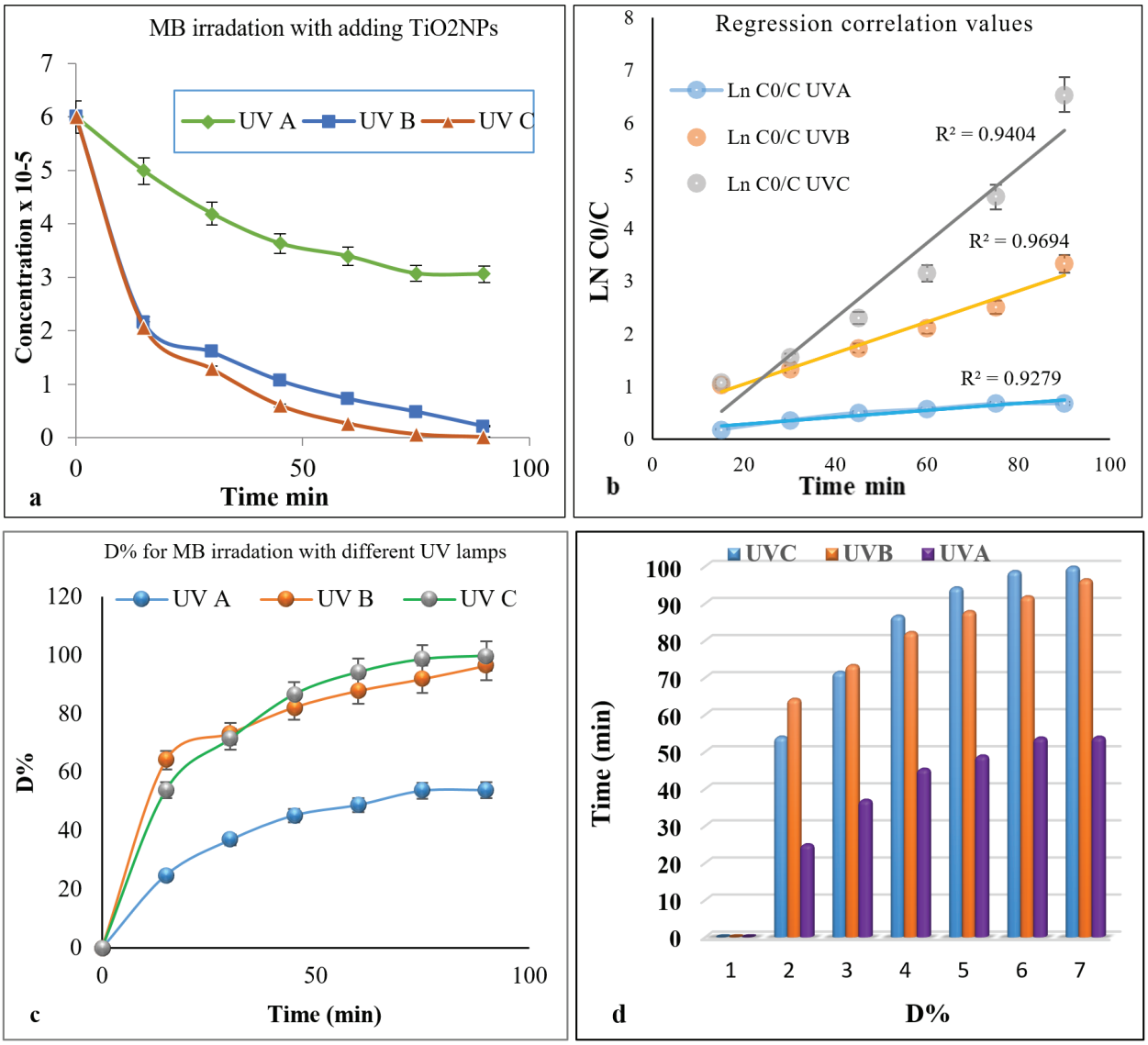

Fig. 11. (**a**) MB Conc. Decrease with time (**b**) Regression correlation values R^2, (**c**) and (**d**) D% for MB irradiation with different UV lamps. all experiments ([MB] = 20 ppm; TiO_2 NPs loading = 0.05g)

or harmless substances. This is particularly useful for treating industrial wastewater and contaminated natural water. The results of the photodegradation process, with loading (0.05g) of TiO_2NPs, indicate the effectiveness of ultraviolet C rays, as they have higher energy and shorter wavelengths. Compared to ultraviolet B and ultraviolet A, this makes them very effective at breaking chemical bonds in methylene blue dye (20 mg L^{-1}, pH=6.4). This indicates their capability in photolysis, as they have a shorter penetration wavelength and high energy level.

5. Acknowledgements

The authors thank the Department of Chemistry, College of Science, University of Baghdad, Baghdad, Iraq.

6. References

[1] N. Joudeh, D. Linke, Nanoparticle classification, physicochemical properties, characterization, and applications: a comprehensive review for biologists, J. Nanobiotechnol., 20 (2022) 262. https://doi.org/10.1186/s12951-022-01477-8.

[2] B. Mekuye, B. Abera, Nanomaterials: An overview of synthesis, classification, characterization, and applications, Nano Select, 4 (2023) 486–501. https://doi.org/10.1002/nano.202300038

[3] R. Griffo, F. Di Natale, M. Minale, M. Sirignano, A. Parisi, C. Carotenuto, Analysis of carbon nanoparticle coatings via wettability, Nanomater., 14 (2024) 301. https://doi.org/10.3390/nano14030301

[4] M. Mohammadi Asl, N. Mansouri, S. A. R. Haji Seyed Mirzahosseini, F. Atabi, Simultaneity comparative evaluation of toluene removal from the air by adsorption and UV semi-degradation-based adsorption procedure, Int. J. Environ. Sci. Technol., 21 (2024) 6677-6694. https://doi.org/10.1007/s13762-024-05503-0

[5] M. M. Asl, F. Atabi, Functionalized graphene oxide with bismuth and titanium oxide nanoparticles for efficiently removing formaldehyde from the air by photocatalytic degradation–adsorption process, J. Anal. Test., 7 (2023) 444-458. https://doi.org/10.1007/s41664-023-00272-0

[6] Y.N. Slavin, J. Asnis, U.O. Häfeli, H. Bach, Metal nanoparticles: Understanding the mechanisms behind antibacterial activity, J. Nanobiotechnol., 15 (2017) 65. https://doi.org/10.1186/s12951-017-0308-z

[7] M. Arjomandi, H. Shirkhanloo, A Review: Analytical methods for heavy metals determination in environment and human samples, Anal. Methods Environ. Chem. J., 2 (2019) 97–126. https://doi.org/10.24200/amecj.v2.i03.73

[8] S. Syamsol Bahri, Z. Harun, S. Khadijah Hubadillah, W. Norhayati Wan Salleh, N. Rosman, N. Hasliza Kamaruddin, F. Hafeez Azhar, N. Sazali, R. Adiba Raja Ahmad, H. Basri, Review on recent advance biosynthesis of TiO2 nanoparticles from plant-mediated materials: characterization, mechanism and application, IOP Conf. Ser. Mater. Sci. Eng., 1142 (2021) 012005. https://doi.org/10.1088/1757-899x/1142/1/012005

[9] P. Sathishkumar, F.L. Gu, Q. Zhan, T. Palvannan, A.R. Mohd Yusoff, Flavonoids mediated 'Green' nanomaterials: A novel nanomedicine system to treat various diseases – Current trends and future perspective, Mater. Lett., 210 (2018) 26–30. https://doi.org/10.1016/j.matlet.2017.08.078

[10] Z. Zahra, Z. Habib, S. Chung, M.A. Badshah, Exposure route of TiO2 nps from industrial applications to wastewater treatment and their impacts on the agro-environment, Nanomater., 10 (2020) 1–22. https://doi.org/10.3390/nano10081469

[11] A.K. Abass, W.N.J. Al Sieadi, A.K.M.A. Al-Sammarraie, Investigation of the electrical, compositional, and magnetic features of hybrid lead oxide nanocomposites, Eurasian Chem. Commun., 4 (2022) 1044–1053. https://doi.org/10.22034/ecc.2022.344547.1479

[12] N. Rousta, M. Aslan, M. Yesilcimen Akbas, F. Ozcan, T. Sar, M.J. Taherzadeh, Effects of

fungal based bioactive compounds on human health: Review paper, Crit. Rev. Food Sci. Nutr., 64 (2023) 7004-7027. https://doi.org/10.1080/10408398.2023.2178379

[13] V. Tadioto, A. Giehl, R.D. Cadamuro, I.Z. Guterres, A.A. dos Santos, S.K. Bressan, L. Werlang, B.U. Stambuk, G. Fongaro, I.T. Silva, S.L. Alves, Bioactive compounds from and against Yeasts in the one health context: A comprehensive review, Ferment., 9 (2023) 363. https://doi.org/10.3390/fermentation9040363

[14] Y. Xie, Q. Peng, Y. Ji, A. Xie, L. Yang, S. Mu, Z. Li, T. He, Y. Xiao, J. Zhao, Q. Zhang, Isolation and identification of antibacterial bioactive compounds from bacillus megaterium L2, Front. Microbiol., 12 (2021) 645484. https://doi.org/10.3389/fmicb.2021.645484

[15] O. Ying Qian, S. Harith, M. Razif Shahril, N. Shahidan, Bioactive compounds in Cucumis melo L. and its beneficial health effect scoping review, Malays. Appl. Biol., 48 (2019) 11-23. https://jms.mabjournal.com/index.php/mab/article/view/1872

[16] A. Rana, K. Yadav, S. Jagadevan, A comprehensive review on green synthesis of nature-inspired metal nanoparticles: Mechanism, application and toxicity, J. Clean. Prod., 272 (2020)122880. https://doi.org/10.1016/j.jclepro.2020.122880

[17] A. Tsakni, A. Chatzilazarou, E. Tsakali, A.G. Tsantes, J. Van Impe, D. Houhoula, Identification of bioactive compounds in plant extracts of greek flora and their antimicrobial and antioxidant activity, Sep. J., 10 (2023) 373. https://doi.org/10.3390/separations10070373

[18] F.M. Vella, R. Calandrelli, D. Cautela, B. Laratta, Natural antioxidant potential of Melon Peels for fortified foods, Foods, 12 (2023) 2523. https://doi.org/10.3390/foods12132523

[19] O. Sytar, I. Smetanska, Bioactive compounds from natural sources (2020, 2021), Molecules, 27 (2022) 1929. https://doi.org/10.3390/molecules27061929

[20] M. Loi, C. Paciolla, A.F. Logrieco, G. Mulè, Plant bioactive compounds in pre- and postharvest management for aflatoxins reduction, Front. Microbiol., 11 (2020) 243. https://doi.org/10.3389/fmicb.2020.00243

[21] M. Kussmann, D.H. Abe Cunha, S. Berciano, Bioactive compounds for human and planetary health, Front. Nutr. 10 (2023) 1193848. https://doi.org/10.3389/fnut.2023.1193848

[22] P.M. Rolim, G.P. Fidelis, C.E.A. Padilha, E.S. Santos, H.A.O. Rocha, G.R. Macedo, Phenolic profile and antioxidant activity from peels and seeds of melon (Cucumis melo L. var. reticulatus) and their antiproliferative effect in cancer cells, Braz. J. Med. Biol. Res., 51 (2018) e6069. https://doi.org/10.1590/1414-431x20176069

[23] A.S. Rini, Y. Rati, R. Fadillah, R. Farma, L. Umar, Y. Soerbakti, Improved photocatalytic activity of ZnO film prepared via green synthesis method using red watermelon rind extract, Evergreen, 9 (2022) 1046–1055. https://doi.org/10.5109/6625718

[24] N. Basavegowda, K.H. Baek, Multimetallic nanoparticles as alternative antimicrobial agents: Challenges and perspectives, Molecules, 26 (2021) 912. https://doi.org/10.3390/molecules26040912

[25] M. Nadeem, M. Navida, K. Ameer, A. Iqbal, F. Malik, M.A. Nadeem, H. Fatima, A. Ahmed, A. Din, A comprehensive review on the watermelon phytochemical profile and their bioactive and therapeutic effects, Korean J. Food Preserv., 29 (2022) 546–576. https://doi.org/10.11002/KJFP.2022.29.4.546

[26] A.S. Rini, H. Adzani, T.S.L. Husain, M.P. Deraf, Y. Rati, Y. Hamzah, Structural and morphological studies of silver nanoparticles prepared using citrullus lanatus rind extract, in: AIP Conf. Proc., Am. Institute Phys. Inc., 2021. https://doi.org/10.1063/5.0037960

[27] W. Chums-ard, D. Fawcett, C.C. Fung, G.E.J. Poinern, Biogenic synthesis of gold nanoparticles from waste watermelon and their antibacterial activity against Escherichia coli and Staphylococcus epidermidis, Int. J. Res. Med. Sci., 7 (2019) 2499. https://doi.

org/10.18203/2320-6012.ijrms20192874

[28] S. Teimoori, H. Shirkhanloo, A.H. Hassani, M. Panahi, N. Mansouri, Rapid extraction of BTEX in water and milk samples based on functionalized multi-walled carbon nanotubes by dispersive homogenized-micro-solid phase extraction, Food Chem., 421 (2023) 136229. https://doi.org/10.1016/j.foodchem.2023.136229

[29] S. Teimoori, H. Shirkhanloo, A.H. Hassani, M. Panahi, N. Mansouri, New extraction of toluene from water samples based on nano-carbon structure before determination by gas chromatography, Int. J. Environ. Sci. Technol., 20 (2023) 6589–6608. https://doi.org/10.1007/s13762-023-04906-9

[30] J. Lee, U. Von Gunten, J.H. Kim, Persulfate-based advanced Oxidation: Critical assessment of opportunities and roadblocks, Environ. Sci. Technol., 54 (2020) 3064–3081. https://doi.org/10.1021/acs.est.9b07082

[31] J. Rakhtshah, H. Shirkhanloo, N. Esmaeili, A rapid extraction of toxic styrene from water and wastewater samples based on hydroxyethyl methylimidazolium tetrafluoroborate immobilized on MWCNTs by ultra-assisted dispersive cyclic conjugation-micro-solid phase extraction, Microchem. J., 170 (2021) 106759. https://doi.org/10.1016/j.microc.2021.106759

[32] Z. Karamzadeh, A novel biostructure sorbent based on CysSB/MetSB@ MWCNTs for separation of nickel and cobalt in biological samples by ultrasound assisted-dispersive ionic liquid- suspension solid phase microextraction, J. Pharm. Biomed. Anal., 172 (2019) 285-294. https://doi.org/10.1016/j.jpba.2019.05.003

[33] A. Faghihi-Zarandi, J. Rakhtshah, B. B. Yarahmadi, A rapid removal of xylene vapor from environmental air based on bismuth oxide coupled to heterogeneous graphene/graphene oxide by UV photo-catalectic degradation-adsorption procedure, J. Environ. Chem. Eng., 8 (2020) 104193. https://doi.org/10.1016/j.jece.2020.104193

[34] A. Romandini, A. Pani, P.A. Schenardi, G.A.C. Pattarino, C. De Giacomo, F. Scaglione, Antibiotic resistance in pediatric infections: Global emerging threats, predicting the near future, Antibiotics, 10 (2021) 393. https://doi.org/10.3390/antibiotics10040393

[35] E.Y. Ahn, S.W. Shin, K. Kim, Y. Park, Facile Green Synthesis of titanium dioxide nanoparticles by upcycling mangosteen (Garcinia mangostana) pericarp extract, Nanoscale Res. Lett., 17 (2022) 40. https://doi.org/10.1186/s11671-022-03678-4

[36] M. Ghosh, P. Chowdhury, A.K. Ray, Photocatalytic activity of aeroxide tio2 sensitized by natural dye extracted from mangosteen peel, Catal., 10 (2020) 917. https://doi.org/10.3390/catal10080917

[37] S. Kumar, W. Ahlawat, G. Bhanjana, S. Heydarifard, M.M. Nazhad, N. Dilbaghi, Nanotechnology-based water treatment strategies, J. Nanosci. Nanotechnol., 14 (2014) 1838–1858. https://doi.org/10.1166/jnn.2014.9050

[38] B. Abebe, H.C.A. Murthy, E. Amare, Summary on adsorption and photocatalysis for pollutant remediation: Mini review, J. Encapsulation Adsorp. Sci., 08 (2018) 225–255. https://doi.org/10.4236/jeas.2018.84012

[39] M.S. Anantha, S. Olivera, C. Hu, B.K. Jayanna, N. Reddy, K. Venkatesh, H.B. Muralidhara, R. Naidu, Comparison of the photocatalytic, adsorption and electrochemical methods for the removal of cationic dyes from aqueous solutions, Environ. Technol. Innov., 17 (2020) 100612. https://doi.org/10.1016/j.eti.2020.100612

[40] S. Teimoori, H. Shirkhanloo, A.H. Hassani, M. Panahi, N. Mansouri, An immobilization of aminopropyl trimethoxysilane-phenanthrene carbaldehyde on graphene oxide for toluene extraction and separation in water samples, Chemosphere, 316 (2023) 137800. https://doi.org/10.1016/j.chemosphere.2023.137800

[41] S. Woo, H. Jung, Y. Yoon, Real-Time UV/VIS spectroscopy to observe photocatalytic degradation, Catal., 13 (2023) 683. https://doi.org/10.3390/catal13040683

[42] S. Alkaykh, A. Mbarek, E.E. Ali-Shattle, Photocatalytic degradation of methylene blue dye in aqueous solution by MnTiO3 nanoparticles under sunlight irradiation, Heliyon, 6 (2020) e03663. https://doi.org/10.1016/j.heliyon.2020.e03663

[43] G. V. Geetha, R. Sivakumar, C. Sanjeeviraja, V. Ganesh, Photocatalytic degradation of methylene blue dye using ZnWO4 catalyst prepared by a simple co-precipitation technique, J. Solgel Sci. Technol., 97 (2021) 572–580. https://doi.org/10.1007/s10971-021-05480-7

[44] T. Nakayama, R. Honda, K. Kuwata, S. Usui, B. Uno, Electrochemical and mechanistic study of reactivities of α-, β-, γ-, and δ-tocopherol toward electrogenerated superoxide in N,N-dimethylformamide through proton-coupled electron transfer, Antioxidants, 11 (2022) 9. https://doi.org/10.3390/antiox11010009

[45] J. Iqbal, B.A. Abbasi, T. Yaseen, S.A. Zahra, A. Shahbaz, S.A. Shah, S. Uddin, X. Ma, B. Raouf, S. Kanwal, W. Amin, T. Mahmood, H.A. El-Serehy, P. Ahmad, Green synthesis of zinc oxide nanoparticles using Elaeagnus angustifolia L. leaf extracts and their multiple in vitro biological applications, Sci. Rep., 11 (2021) 20988. https://doi.org/10.1038/s41598-021-99839-z

[46] X. Jaramillo-Fierro, J. Ramón, E. Valarezo, Cyanide removal by $ZnTiO_3/TiO_2/H_2O_2$/UVB system: A theoretical-experimental approach, Int. J. Mol. Sci., 24 (2023) 16446. https://doi.org/10.3390/ijms242216446

[47] R. Ahmadiasl, G. Moussavi, S. Shekoohiyan, F. Razavian, Synthesis of Cu-doped TiO2 nanocatalyst for the enhanced photocatalytic degradation and mineralization of gabapentin under UVA/LED irradiation: Characterization and photocatalytic activity, Catal., 12 (2022) 1310. https://doi.org/10.3390/catal12111310

[48] X. Li, Y. Gao, H. Xiong, Z. Yang, The electrochemical redox mechanism and antioxidant activity of polyphenolic compounds based on inlaid multi-walled carbon nanotubes-modified graphite electrode, Open Chem., 19 (2021) 961–973. https://doi.org/10.1515/chem-2021-0087

[49] R.D. Desiati, M. Taspika, E. Sugiarti, Effect of calcination temperature on the antibacterial activity of TiO_2/Ag nanocomposite, Mater. Res. Express., 6 (2019) 095059. https://doi.org/10.1088/2053-1591/ab155c

[50] D.R. Eddy, S.N. Ishmah, M.D. Permana, M.L. Firdaus, I. Rahayu, Y.A. El-Badry, E.E. Hussein, Z.M. El-Bahy, Photocatalytic phenol degradation by silica-modified titanium dioxide, Appl. Sci., 11 (2021) 9033. https://doi.org/10.3390/app11199033

[51] M. M. Eskandari, B. Kalantari, Dispersive liquid-liquid microextraction based on task-specific ionic liquids for determination and speciation of chromium in human blood, J. Anal. Chem., 70 (2015) 1448-1455. https://doi.org/10.1134/S1061934815120072

[52] K.E. Al Ani, A.E. Ramadhan, W.N. Al Sieadi, Fourier-transform infrared spectroscopic study of plasticization effects on the photodegradation of poly(fluorostyrene) isomers films, J. Vinyl Add. Technol., 24 (2018) 75–83. https://doi.org/10.1002/vnl.21529

[53] W.B. Baker, A.B. Parthasarathy, D.R. Busch, R.C. Mesquita, J.H. Greenberg, A.G. Yodh, Modified beer-lambert law for blood flow, Biomed. Opt. Express, 5 (2014) 4053. https://doi.org/10.1364/boe.5.004053

[54] A.S. Rini, Y. Rati, R. Dewi, S. Putri, Investigating the influence of precursor concentration on the photodegradation of methylene blue using biosynthesized ZnO from pometia pinnata leaf extracts, Baghdad Sci. J., 20 (2023) 2532–2539. https://doi.org/10.21123/bsj.2023.9176

[55] S.A. Mousa, S. Tareq, E.A. Muhammed, Studying the photodegradation of Congo red dye from aqueous solutions using bimetallic Au-Pd/TiO_2 photocatalyst, Baghdad Sci. J., 18 (2021) 1261–1268. https://doi.org/10.21123/BSJ.2021.18.4.1261